Catalysis Today 323 (2019) 123–128

Contents lists available at ScienceDirect

Catalysis Today

journal homepage: www.elsevier.com/locate/cattod

Promotion of Pd nanoparticles by Fe and formation of a Pd_3Fe intermetallic alloy for propane dehydrogenation

Ce Yang[a], Zhenwei Wu[b], Guanghui Zhang[b,*], Huaping Sheng[d], Jun Tian[d], Zhengli Duan[d], Hyuntae Sohn[a], A. Jeremy Kropf[a], Tianpin Wu[c], Theodore R. Krause[a], Jeffrey T. Miller[a,b,*]

[a] Chemical Science and Engineering Division, Argonne National Laboratory, Lemont, IL, 60439, USA
[b] Davidson School of Chemical Engineering, Purdue University, 480 Stadium Mall Drive, West Lafayette, IN, 47907, USA
[c] Advanced Photon Source, Argonne National Laboratory, Lemont, IL, 60439, USA
[d] Center for Nanoscale Materials, Argonne National Laboratory, Lemont, IL, 60439, USA

ARTICLE INFO

Keywords:
Pd_3Fe nanoparticles
X-ray absorption
X-ray diffraction
Propane dehydrogenation

ABSTRACT

Silica supported Pd (~2 nm), Pd_3Fe (~2 nm) and Pd_3Fe_large (~12 nm) catalysts were synthesized and tested for propane dehydrogenation at 510 °C. At the 10% conversion, Pd and Pd_3Fe catalysts exhibited propylene selectivity of 45% and 94%, respectively. Moreover, the latter showed a turnover rate (TOR) of 0.2 s^{-1}, which is five times higher than that of the Pd catalyst (0.04 s^{-1}). Pd K edge XAS, XRD, and CO adsorbed IR were used to characterize the geometric structure of the catalysts. By combined comparison of XRD and XAS spectra of Pd_3Fe and Pd_3Fe_large catalysts, we successfully identified the crystalline phase in the 2 nm Pd_3Fe catalyst. The CO adsorbed IR suggests that the formation of Pd_3Fe breaks the ensemble of Pd, which is responsible for the increase of selectivity. The Pd L edge XAS was used to characterize the electronic structure of the catalysts. The Pd_3Fe catalyst exhibits an increase of the edge energy compared with the Pd catalyst, which indicates the change of d-band structure in the bimetallic catalyst. The change in the electronic structure is likely the reason for the increase in TOR.

1. Introduction

Light hydrocarbons, such as ethane, propane and butane, are abundantly distributed in shale natural gas, and can be used for production of fuels and chemicals through dehydrogenation, oligomerization and other functionalization reactions [1,2]. There are two major types of alkane dehydrogenation catalysts: Pt-based bimetallics and CrO_x. The former has higher activity, moderate selectivity and stability [3,4]; while the latter has higher selectivity, but is poorly active and stable [1,5,6]. Other noble metal catalysts, for example Pd, are poorly selective with high yield of methane, and they rapidly deactivate due to coke formation. It has long been known that the addition of promoter significantly enhances the performance of Pt catalysts. Addition of an inert second metal such as Sn, Ga, Zn or In enhances the selectivity as well as activity [4,7–11]. Many studies have suggested geometric and electronic effects are decisive for high selectivity in promoted Pt dehydrogenation catalysts [2,3,12,13,14,15]. Most often, the electronic effects by the promotor metal atoms are considered to be responsible for the improved selectivity of the catalysts [16,17]. Recently, with the help of using synchrotron X-ray diffraction to determine the alloy structure in dehydrogenation catalysts, it has been suggested that a geometric effect, i.e., isolation of active site by the second metal, is the primary reason for the enhancement of selectivity and suppression of the structural-sensitive C—C hydrogenolysis and coking reactions. For example, improved dehydrogenation performances have been demonstrated for the AuCu type intermetallics β_1PdZn, Pt_1Zn_1, CsCl type PdIn, and Cu_3Au type Pt_3In [18–20]. In addition, a recent resonant inelastic X-ray scattering study on Pt_1Zn_1 intermetallic alloy showed that the energy of the filled Pt valence 5d orbitals decrease and the energy of the unfilled Pt 5d orbitals increase upon bonding with Zn [18]. Thus, the dominant electronic effect was a change in the energy of the filled and unfilled 5d orbitals, rather than a change in the number of electrons as is generally suggested in the Pt-Sn catalysts [19,21,23]. Lowering of the energy of the filled Pt 5d valence orbitals results in the decrease of Pt-adsorbate bond energy leading to a decrease in the metal adsorbate bond energy and reactant surface coverage.

In this manuscript Pd and Pd_3Fe intermetallic alloy nanoparticles (NPs) are prepared and tested for propane dehydrogenation. The Pd_3Fe catalyst has higher selectivity for production of olefins with improved stability compared with Pd NPs of the same size. The catalysts were

* Corresponding authors at: Davidson School of Chemical Engineering, Purdue University, 480 Stadium Mall Drive, West Lafayette, IN, 47907, USA.
E-mail addresses: zhan2739@purdue.edu (G. Zhang), mill1194@purdue.edu (J.T. Miller).

https://doi.org/10.1016/j.cattod.2018.07.043
Received 11 January 2018; Received in revised form 3 July 2018; Accepted 15 July 2018
Available online 17 July 2018

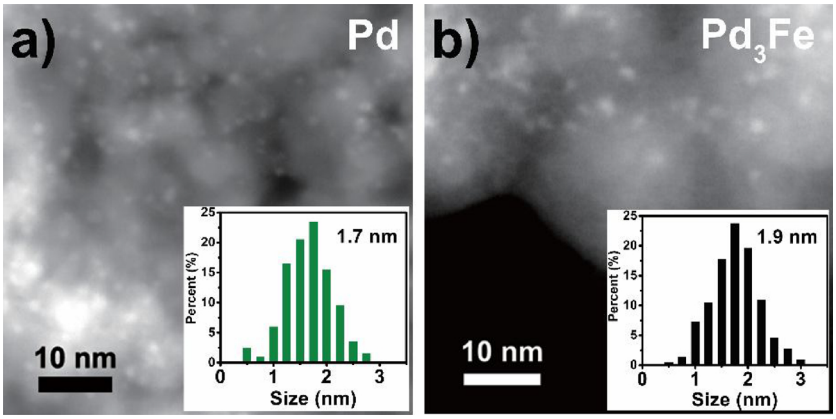

Fig. 1. STEM images of a) Pd/SiO_2 and b) Pd_3Fe/SiO_2 catalysts. The insets are particle size distribution of corresponding samples.

characterized by Pd K-edge and L-edge X-ray absorption spectroscopy (XAS), synchrotron X-ray diffraction (XRD), Infrared (IR) spectroscopy of adsorbed CO and Scanning transmission electron microscopy (STEM). In the Pd_3Fe catalyst, the Pd ensembles are broken by inactive Fe atoms, which is believed to be the primary reason for the improved selectivity and stability. Moreover, the changes in Pd L edge X-ray absorption near edge structure (XANES) suggest changes in the electronic structures; however, these are not likely large enough to account for the large change in dehydrogenation selectivity.

2. Results

The Pd catalyst was synthesized by strong electrostatic adsorption and Pd_3Fe catalysts were prepared by incipient wetness impregnation as described in the experimental section of supplemental information (SI). As can be seen in the STEM images, Fig. 1, NPs with average size of 1.7 nm were obtained in the Pd catalyst prepared by strong electrostatic adsorption of $Pd(NH_3)_4(NO_3)_2$ on SiO_2 in strongly basic pH with NH_4OH. For the Pd_3Fe catalyst, Fe was firstly added to silica by impregnation of $Fe(NO_3)_3{\cdot}xH_2O$ with citric acid. Addition of NH_4OH to the $Fe(NO_3)_3$ solution leads to precipitation of iron hydroxide-oxide, which is not suitable for impregnation. However, addition of citric acid prior to addition of NH_4OH leads to a clear Fe-citrate complex, which can be impregnated on silica to get Fe/SiO_2 with uniform dispersion. Subsequent impregnation of a basic solution of $Pd(NH_3)_4(NO_3)_2$ on Fe/SiO_2 gives NPs with an average size of 1.9 nm. Under identical conditions, impregnation of $Pd(NH_3)_4Cl_2$ on $Fe\text{-}SiO_2$ leads to large NP's with an average size of 12 nm (Figure S1). The presence of Cl on the catalyst appears to give significantly larger NPs than that without Cl.

The catalysts were characterized by *in-situ* X-ray absorption spectroscopy. After reduction in H_2, the X-ray absorption near edge spectra (XANES) at Pd K edge (24,350 eV) indicates that the shape as well as the edge energy and white line intensity of the three samples are similar, indicating Pd is fully reduced to metallic in all samples (Figure S2). Small changes in the shape of the XANES of the Pd_3Fe catalysts compared to Pd suggest that bimetallic NPs form. The magnitudes and imaginary parts of the k^2-weighted extended X-ray absorption spectra (EXAFS) are shown in Fig. 2. Fig. 2a and c show spectra characteristic of metallic Pd NP, while those of the Pd_3Fe catalysts shown in Fig. 2b and d are significantly different. The EXAFS spectra of Pd_3Fe show scattering from metallic Fe as well as Pd. The Pd K edge EXAFS of Pd_3Fe_large is very similar to that of the small particle except that the intensity of the magnitude of the FT-EXAFS is higher (Fig. 3) consistent with a larger particle size. The EXAFS, both magnitude and imaginary

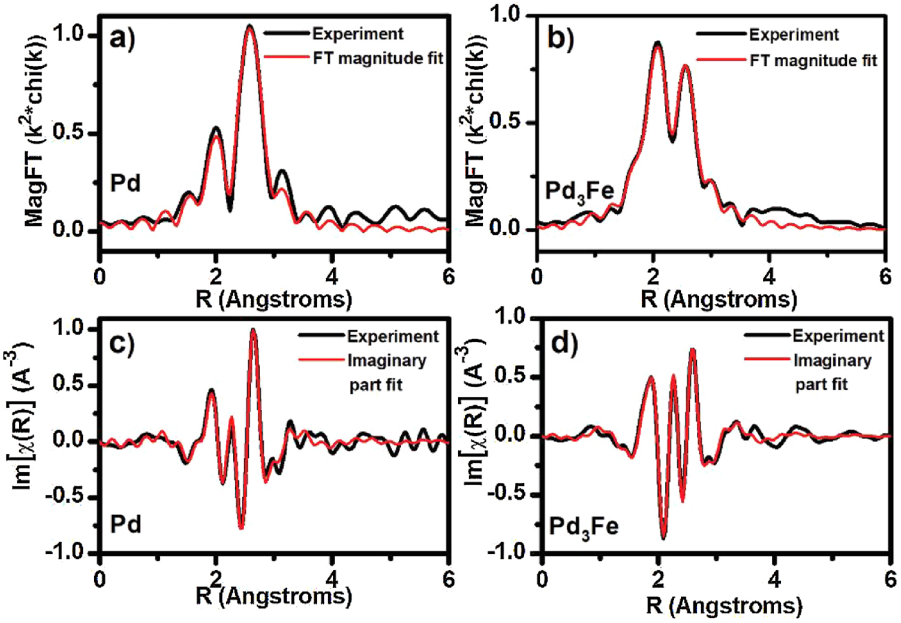

Fig. 2. a–b) Magnitude of fitted and experimental Fourier-transformed EXAFS (FT-EXAFS) spectra for Pd and Pd_3Fe catalysts. c–d) Imaginary part of fitted and experimental FT-EXAFS spectra for Pd and Pd_3Fe catalysts.

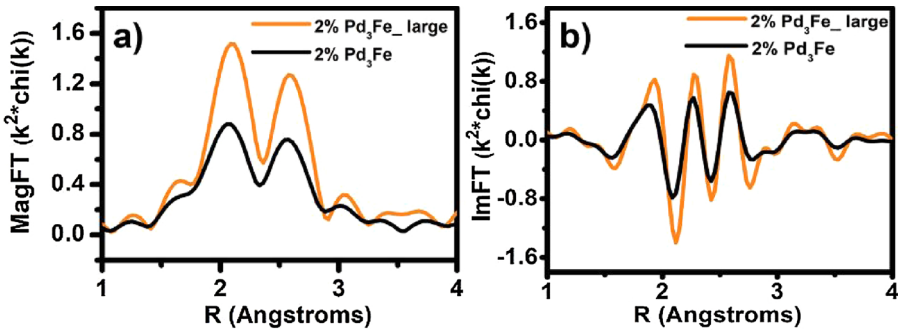

Fig. 3. a) Magnitude and b) imaginary part of FT-EXAFS patterns of Pd_3Fe_large and Pd_3Fe catalysts.

Table 1
Pd K-edge EXAFS fitting parameter and Pd L edges energy for Pd-Fe catalysts (k^2: Δk = 3–12 $Å^{-1}$ and ΔR = . 1.5–3.0 Å)

Sample	Scattering path	Coordination number	Bond distance (Å)	Debye Waller factor $\Delta\sigma^2$ (10^{-3})	Pd L3 edge energy (eV)	Pd L2 edge energy (eV)
Pd	Pd-Pd	6.6	2.75	9.0	3173.6	3330.6
Pd_3Fe	Pd-Fe	2.6	2.61	8.6	3173.8	3331.0
	Pd-Pd	4.9	2.71	9.0		
Pd_3Fe_large	Pd-Fe	3.5	2.63	6.3	3174.3	3331.2
	Pd-Pd	7.0	2.72	7.5		

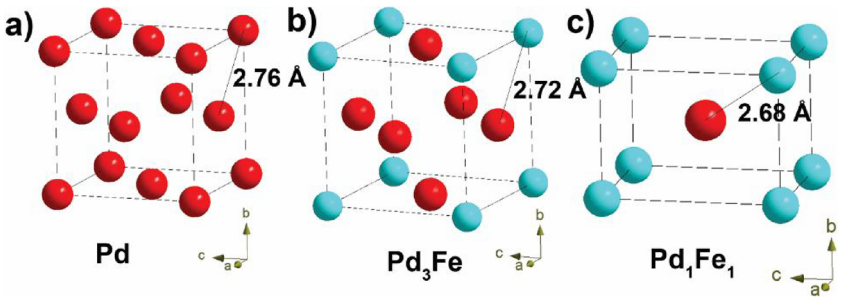

Fig. 4. Crystal structure of a) Pd, b) Pd_3Fe and c) Pd_1Fe_1 intermetallic compound phases [28–30].

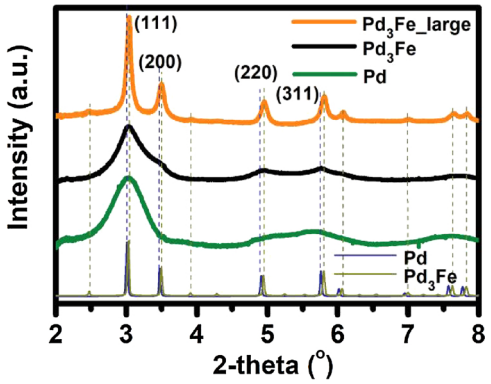

Fig. 5. XRD of Pd, Pd_3Fe and Pd_3Fe_large catalysts.

part, of the FT-EXAFS were fit and the results are given in Table 1. The quality of the fits is shown in Fig. 2. The coordination number of the Pd catalyst is 6.6 and the Pd-Pd bond length is 2.75 Å, consistent with small metallic Pd NPs. Estimating the NP size from the coordination numbers gives an approximate size of 1.9 nm consistent with the STEM results [25].

In the Pd_3Fe catalysts, the fits were poor using only Pd-Pd scattering. Addition of a Pd-Fe scattering path gave good fits. The Pd-Pd distance was shorter than in the Pd NP despite the similar size. The Pd-Fe bond distance was about 2.62 Å, which is about the sum of the radii of metallic Pd and Fe, i.e. (2.75 + 2.48)/2 = 2.615 Å. The ratio of the coordination number of Pd-Pd to Pd-Fe was approximately 2 for both Pd_3Fe catalysts, which is in line with that of the crystal structure of Pd_3Fe (Fig. 4). The Fe K-edge (7112 eV) XANES of the Pd_3Fe catalyst (Figure S3a and S3b) indicates that most of the Fe is present in the Fe (II) oxidation state [24,26]. In our previous studies, Fe(II)/SiO_2 shows much lower (two orders magnitude) dehydrogenation activity under our reaction conditions, so the unreduced Fe present in the bimetallic Pd_3Fe catalyst should be considered as inactive [24]. The EXAFS indicates that much of the Fe has O bonds. There is a small higher shell peak between about 2–3 Å (uncorrected distance) in the magnitude of the FT-EXAFS. The small size of the peak and the potential overlap with Fe—O—Fe bonds from Fe oxide, prevented fitting of Fe-Pd scattering in

Table 2
in situ XRD results of the three catalysts.

Sample	2-theta angles of [111] planes	Lattice parameters (Å)	Particle size (nm)
Pd	3.015	3.865	1.7
Pd_3Fe	3.046	3.826	1.9
Pd_3Fe_large	3.039	3.835	12

Data taken at 35 °C in He after reduction with H_2 at 550 °C.

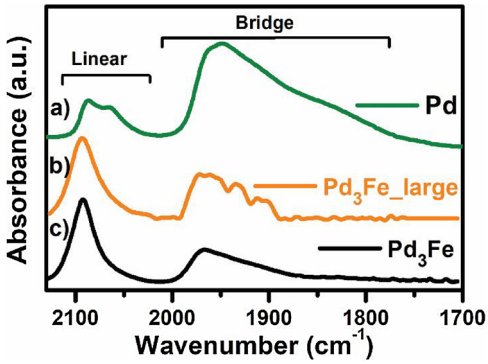

Fig. 6. IR spectra of adsorbed CO on a) Pd, b) Pd_3Fe_large and c) Pd_3Fe catalysts. The spectra were measured after saturation and subsequent purging with helium at room temperature.

Table 3
Ratio of the peak area of bridge to linear-bonded CO by DRIFTS spectroscopy.

Sample	Bridging:Linear ratio
Pd	6.7 : 1
Pd_3Fe	0.9 : 1
Pd_3Fe_large	0.9 : 1

the alloy. In summary, the XAS results indicate the formation of bimetallic Pd-Fe NPs; however, EXAFS is a local characterization and does not determine the crystal structure. To investigate the crystal phase of the NPs, diffraction is needed.

In situ synchrotron X-ray diffraction (XRD) has been previously shown to be possible on NPs with 2 nm size [4,13,27]. The XRD patterns of Pd and Pd_3Fe catalysts along with the simulated patterns of bulk Pd and Pd_3Fe phases are shown in Fig. 5. The peaks for both Pd_3Fe and Pd catalysts are broad, consistent with their small particle sizes. For the Pd catalyst, the position of maximum peak is observed at 3.01°, corresponding to the simulated Pd (111) peak, which indicates the Pd species is monometallic. The (200) peak, however, merges into the (111) peak due to the small particle size [27]. Also distorted are the peaks at higher 2-thetas. The XRD pattern of Pd_3Fe is similar to Pd except for several minor peaks and a small shift in the peak position (as can be seen from the simulated pattern in Fig. 5). Fig. 5 also shows the XRD peaks of the larger (about 12 nm) Pd_3Fe catalyst. With the larger size, sharp diffraction peaks are recorded and precise peak shifts can be determined. The peaks are shifted compared to monometallic Pd and the position of the (111), (200) and (220) peaks are 3.04, 3.50 and 4.96°, respectively, which corresponds to the simulated pattern of Cu_3Au type Pd_3Fe intermetallic phase. Even the small superlattice peaks characteristic of the Pd_3Fe phase are visible at 2θ of 2.49, 3.92 and 6.99°, which confirms the Pd_3Fe phase in the sample. From the peak positions of the XRD, the unit cell size was determined for the Pd and

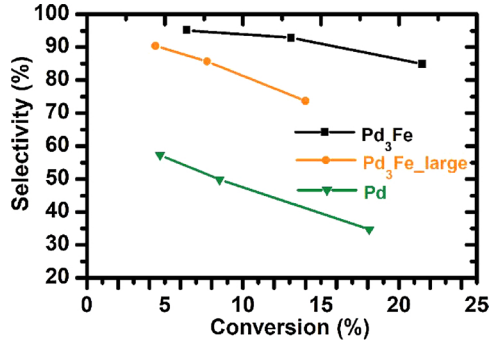

Fig. 8. Propylene selectivity vs conversion of Pd_3Fe, Pd and Pd_3Fe_large catalysts (reaction conditions: 180 mL/min of 1.5% C_3H_8, 1.5% H_2 balanced in Ar at 1 atm and 510 °C).

the two Pd_3Fe NPs. The results and corresponding particle sizes are shown in Table 2. The lattice parameter decreases from 3.865 Å in Pd catalyst to 3.826 Å in Pd_3Fe catalyst, in line with the decrease in the lattice upon alloying with Fe. Moreover, a slight increase of the lattice parameter from 3.826 to 3.835 between Pd_3Fe and Pd_3Fe_large catalysts also agrees with the size effect, where the contraction of lattice is observed when the particle size decreases below 30 Å [25]. Therefore, along with the results obtained from XAS where both Pd_3Fe samples have the same ratio of CN of Pd-Pd to Pd-Fe paths as 2, confirm the phases in both samples as Pd_3Fe.

In situ IR spectra of chemisorbed CO on Pd and Pd_3Fe catalysts are shown in Fig. 6. As is well studied, the vibration band between 1700 cm^{-1} and 2000 cm^{-1} represents the bridge bonded CO while the vibration band between 2150 cm^{-1} and 2050 cm^{-1} represent the linearly bonded CO. For the monometallic Pd sample, the bridge-bonded broad band between 2000 cm^{-1} and 1700 cm^{-1} is the largest peak. The ratio of peak areas of Pd (bridge-to-linear ratio) is 6.7, consistent with previous studies of small Pd (2 nm) catalysts, Fig. 6a [3,13]. After alloying with Fe, the IR spectrum of absorbed CO shows predominantly linear-bonded bands between 2050 cm^{-1} and 2150 cm^{-1} with bridge-to-linear ratio of 0.9, Fig. 6c. The IR spectrum of CO adsorbed Pd_3Fe_large also shows predominantly linear-bonded CO with a similar bridge-to-linear ratio as shown in Table 3 and Fig. 6b [22]. Because of the larger size of the latter catalyst, the noise in the absorption band between 2000 cm^{-1} and 1900 cm^{-1} originates from the low CO uptake. In addition to a shift from bridge to linear bonded CO in the diffuse reflectance infrared Fourier transform spectroscopy (DRIFTS), there is a change in the type of bridge bonded CO. The band centered about 1850 cm^{-1} in the Pd catalyst, which represents the 3-fold hollow site [31] is completely absent in the Pd_3Fe NP's. For the latter, there is bridge bonded − CO occurs at about 1950 cm^{-1} [32]. Thus, in both Pd_3Fe catalysts the IR spectra indicate there are few 3-fold Pd ensembles remaining.

Electronic effects are often thought to be essential to the promotion of high selectivity in Pt dehydrogenation catalysts [33,34]. For Pd, one

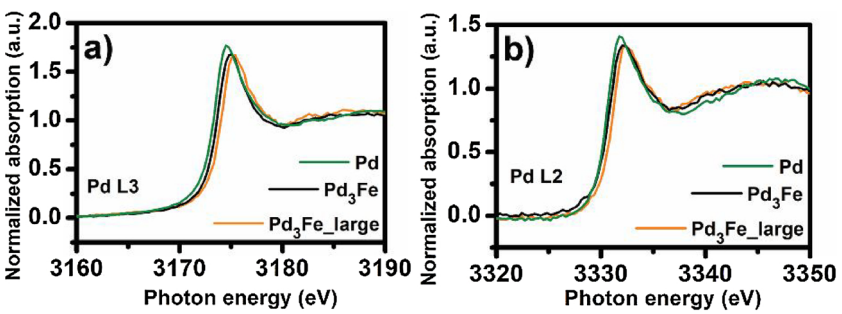

Fig. 7. a) Pd L3 edge (3173 eV) spectra from 3165 to 3180 eV and b) Pd L2 edge (3330 eV) spectra from 3325 to 3340 eV of Pd, Pd_3Fe and Pd_3Fe_large catalysts.

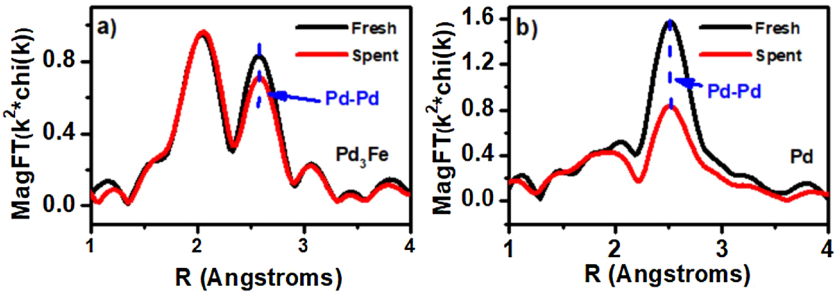

Fig. 9. FT-EXAFS of fresh and spent catalysts of a) Pd_3Fe and b) Pd.

generally measures the K-edge XANES spectra, which is the 1 s to 5p transition. However, the unfilled 5p orbitals have higher energy than the valence 4d orbitals, and thus the K-edge XANES are not indicative of the electronic changes in Pd that are responsible for the catalytic properties. The Pd L-edge XANES spectra (2p to 4d orbital transition) are sensitive to the energy and provide information of the energy of the valence 4d orbital. Fig. 7a and b show the Pd L_3 and L_2 XANES, respectively, for the Pd and Pd_3Fe catalysts. The L_3 edge energy of Pd_3Fe (3173.8 eV) is 0.2 eV higher in energy than Pd (3173.6 eV). There is a larger shift of edge position, 0.5 eV, in Pd_3Fe_large NP's (3174.3 eV) compared to small Pd NP's [35]. Similarly, at the L_2 edge, the XANES energy of Pd is 3330.6 eV, and Pd_3Fe and Pd_3Fe_large are 3331.0 and 3331.2 eV, respectively, suggesting an increase in energy of the Pd unfilled 4d states upon alloying with Fe.

The catalysts were then tested at 1 atm and 510 °C in a mixture of 1.5% H_2, 1.5% C_3H_8 and 97% Ar for propane dehydrogenation. To test the dehydrogenation selectivity under sever reaction conditions, H_2 was co-fed to promote the hydrogenolysis side reaction. The C_3H_6 selectivity was greatly enhanced after alloying Pd with Fe. At the C_3H_8 conversion of 10%, the Pd catalyst showed a C_3H_6 selectivity of about 45%, while the Pd_3Fe and Pd_3Fe_large catalysts each showed an overall C_3H_6 selectivity of 94% and 80%. At a higher conversion of 20%, the Pd_3Fe catalyst had a C_3H_6 selectivity of 85%; while Pd decreased to 32% (Fig. 8 and S5). The side products are methane, ethane, ethylene and coke. The Pd_3Fe and Pd_3Fe_large catalysts each shows initial TOR as 0.2 and 0.3 s^{-1}, while Pd catalyst shows an initial TOR of merely 0.04 s^{-1} (Table S1). Moreover, after 5 h on stream, the activity of Pd catalysts dropped to only 8% of its original activity; while the Pd_3Fe catalysts kept 50% of its initial activity (Figure S4).

To investigate the origin of deactivation, we performed in situ XAS experiments for both Pd and Pd_3Fe catalysts (Fig. 9). For the Pd catalyst, we observed a significant change in the FT-EXAFS of the spent catalyst. EXAFS fitting results of the spent catalyst suggest the presence of both Pd-C and Pd-Pd bonds. In particular, the CN of Pd-Pd path has dropped from 6.6 to 3.9, and the CN of Pd-C is 2.4 suggesting the formation of PdCx. On the contrary, for the Pd_3Fe catalyst, the FT-EXAFS of spent catalyst shows little difference compared with that of fresh catalyst. (Table S2) Therefore, incorporation of Fe helps the coking resistance and provides the Pd_3Fe catalyst with enhanced stability.

3. Discussion

The XRD results suggest that the Pd_3Fe_large sample has a Pd_3Fe intermetallic structure. The XANES, EXAFS, bond distances, ratios of Pd-Pd to Pd-Fe coordination numbers and infrared spectra of this sample, are all very similar to the Pd_3Fe catalyst. Therefore, we confirmed the Au_3Cu type Pd_3Fe phase in the 1.9 nm catalyst. The STEM images show that both Pd and Pd_3Fe catalysts are similar in size. However, their catalytic performances are significantly different. As is well known, the dehydrogenation selectivity of Pd is poor and deactivation is fast [3,36,7,9,37], As a result, Pd is seldom studied for alkane dehydrogenation. Improvements in olefin selectivity to Pt dehydrogenation catalysts are thought to be dominated by changes in the electronic properties of the 5d orbitals and are generally described as an increase in the number of 5d electrons donated from the Sn 4p orbitals for example [38,39]. However, the orbital symmetries of d and p orbitals are orthogonal and little overlap and weak bonding is expected. Thus, transfer of the Sn 4p electrons to Pt is likely small. While geometric effects also are often suggested [40,41], there is little experimental evidence that the structure or surface has smaller ensembles correlating with selectivity.

Unlike Pd, Pd_3Fe has high olefin selectivity. The shifts in the L edge XANES are small, about 0.2 eV, and not likely enough to modify Pd to perform like Pt, and especially the high selectivity typical of Pt_3Sn. Further evidence that electronic effects do not dominate the selectivity are comparison of the large and small Pd_3Fe. The electronic change in the larger particles is greater than that in the smaller particle; however, the selectivity is lower. If the increase in the XANES energy of the small Pd_3Fe compared to Pd correlated with its selectivity, then further increases should give even higher selectivity, which is not observed. Thus, while alloy formation with Fe does lead to changes in the energy of the empty Pd 4d orbitals, the change in selectivity is likely due to other factors. IR shows that the surface has few Pd ensembles in the Pd_3Fe catalyst, and those surface Pd atoms that bridge bond CO are not effective for alkane hydrogenolysis. The Pd_3Fe structure (Fig. 4) is similar to that of Pt_3Sn and has similarly high olefin selectivity [38]. Although there are adjacent Pd atoms in Pd_3Fe there are no large ensembles, and few 3-fold Pd sites [31]. Thus, it appears that high selectivity can be obtained for structure with two or even three adjacent Pd atoms. While full site isolation is not necessary, the selectivity of PdZn [27] and PdIn [13] were higher than that for these Pd_3Fe. The dehydrogenation selectivity of Pd_3Fe is consistent with the hypothesis that site isolation of the active site by inactive metal atoms is responsible for high olefin selectivity. In addition, structures with two active atoms have good olefin selectivity, although not as high as structures as with completely isolated active sites. Furthermore, if a noble metal with poor selectivity, like Pd, can demonstrate high olefin selectivity, then other poorly selective noble metals may also be possible if the proper intermetallic structure can be synthesized.

While it appears that electronic changes are not the dominant factor for determination of selectivity, the Pd L-edge XANES shows electronic effects do occur upon alloy formation. The influence of electronic effects may increase the TOR. In our previous work, we have demonstrated that, for $Fe(0)/SiO_2$ catalyst, upon exposure to propane, the metallic Fe catalyzes the C—C cleavage and generates coke at very high rate (43 h^{-1}) [24]. As a result, $Fe(0)/SiO_2$ deactivates in few seconds. Therefore, we considered Fe as inactive for propane dehydrogenation. The TOR of Pd_3Fe is five times that of Pd, 0.2 s^{-1} and 0.04 s^{-1} at 510 °C, respectively. The TOR further increases to 0.3 s^{-1} in the Pd_3Fe_large catalyst. Similar increases in TOR have been reported for PdZn, PdIn, Pt_3In and Pt_1Zn_1 intermetallic alloys [3,11,13,18]. It has been proposed that the increase in the L-edge XANES is due to alloy formation. In addition to this increase, there is a corresponding

decrease in the energy of the filled d orbitals, which have recently been measured [18]. If the increase in the Pd L-edge XANES represents a similar decrease in the energy of the filled 4d orbitals of Pd, then Pd-adsorbate bonds will be weaker in Pd_3Fe than Pd, since the energy of the unfilled adsorbate orbitals is higher in energy that the Pd 4d's. As the energy of the Pd 4d orbitals decrease, chemisorption energies will decrease. Thus, Pd-C and Pd-H bonds will be weaker, desorb more easily and result in a faster turnover of the active site. Furthermore, with lower chemisorption energies, one would also expect lower surface coverage of reactants and products, perhaps leading to lower deactivation rates [42,43]. While electronic changes are not thought to be responsible for the large changes in olefin selectivity, they are important to the performance, i.e., rates and stability.

4. Conclusion

2 nm size Pd_3Fe catalysts show have high olefin selectivity for propane dehydrogenation; while monometallic Pd is poorly selective. The electronic modification of the Pd 4d orbitals as measured by changes in the Pd L-edge XANES is likely too small to account for the large changes in selectivity. In addition, larger 12 nm Pd_3Fe_large NP's with even large shifts in the L-edge XANES are less selective; thus there is no correlation between the electronic effects and selectivity. The IR spectrum of Pd_3Fe suggests that there are few surface 3-fold Pd hollow sites suggesting few surface ensembles capable of hydrogenolysis. While there are three adjacent Pd atoms in Pd_3Fe, these show little tendency for hydrogenolysis. The results of this study are consistent with the hypothesis that site isolation of the active metal by inactive atoms is likely responsible for the high olefin selectivity. While electronic effects are not thought to strongly influence the selectivity, there is a correlation between the TOR and change in the Pd L-edge XANES. The shift of L-edge XANES energy implies a corresponding decrease in the energy of the filled Pd 4d orbitals, weaker adsorbate bond energies, lower reactant surface coverages and higher TORs.

Acknowledgements

Z.W., G.Z. and J.T.M. were supported in part by the National Science Foundation under Cooperative Agreement No. EEC-1647722. Any opinions, findings, conclusions, or recommendations expressed in this material are those of the authors and do not necessarily reflect the views of the National Science Foundation. Use of the Advanced Photon Source was supported by the U.S. Department of Energy, Office of Basic Energy Sciences, under contract no. DEAC02-06CH11357. MRCAT operations, beamline 10-BM, are supported by the Department of Energy and the MRCAT member institutions. The authors also acknowledge the use of beamline 11-ID-C.

Appendix A. Supplementary data

Supplementary material related to this article can be found, in the online version, at doi:https://doi.org/10.1016/j.cattod.2018.07.043.

References

[1] C.A. Gartner, A.C. van Veen, J.A. Lercher, Chemcatchem 5 (11) (2013) 3196–3217.
[2] J.J.H.B. Sattler, J. Ruiz-Martinez, E. Santillan-Jimenez, B.M. Weckhuysen, Chem. Rev. 114 (20) (2014) 10613–10653.
[3] D.J. Childers, N.M. Schweitzer, S.M.K. Shahari, R.M. Rioux, J.T. Miller, R.J. Meyer, J. Catal. 318 (2014) 75–84.
[4] Z.X. Ma, Z.W. Wu, J.T. Miller, Jove-J. Vis. Exp. (2017) 125.
[5] J. Baek, H.J. Yun, D. Yun, Y. Choi, J. Yi, ACS Catal. 2 (9) (2012) 1893–1903.
[6] M. Hoang, J.F. Mathews, K.C. Pratt, J. Catal. 171 (1) (1997) 320–324.
[7] V. Galvita, G. Siddiqi, P.P. Sun, A.T. Bell, J. Catal. 271 (2) (2010) 209–219.
[8] J.Y. Shen, J.M. Hill, R.M. Watwe, B.E. Spiewak, J.A. Dumesic, J. Phys. Chem. B 103 (19) (1999) 3923–3934.
[9] A.W. Hauser, P.R. Horn, M. Head-Gordon, A.T. Bell, Phys. Chem. Chem. Phys. 18 (16) (2016) 10906–10917.
[10] Z. Nawaz, Rev. Chem. Eng. 31 (5) (2015) 413–436.
[11] E.C. Wegener, Z.W. Wu, H.T. Tseng, J.R. Gallagher, Y. Ren, R.E. Diaz, F.H. Ribeiro, J.T. Miller, Catal. Today 299 (2018) 146–153.
[12] Z. Yan, Y.X. Yao, D.W. Goodman, Catal. Lett. 142 (6) (2012) 714–717.
[13] Z. Wu, E.C. Wegener, H.T. Tseng, J.R. Gallagher, J.W. Harris, R.E. Diaz, Y. Ren, F.H. Ribeiro, J.T. Miller, Catal. Sci. Technol. 6 (18) (2016) 6965–6976.
[14] M. Boudart, A. Aldag, J.E. Benson, N.A. Dougharty, C. Girvin Harkins, J. Catal. 6 (1966) 92–99.
[15] H. Lieske, A. Sárkány, J. Völter, Appl. Catal. 30 (1987) 69–80.
[16] A. Iglesias-Juez, A.M. Beale, K. Maaijen, T.C. Weng, P. Glatzel, B.M. Weckhuysen, J. Catal. 276 (2010) 268–279.
[17] L. Nykänen, K. Honkala, J. Phys. Chem. C 115 (19) (2011) 9578–9586.
[18] V.J. Cybulskis, B.C. Bukowski, H.T. Tseng, J.R. Gallagher, Z.W. Wu, E. Wegener, A.J. Kropf, B. Ravel, F.H. Ribeiro, J. Greeley, J.T. Miller, ACS Catal. 7 (6) (2017) 4173–4181.
[19] P. Glatzel, J. Singh, K.O. Kvashnina, J.A. van Bokhoven, J. Am. Chem. Soc. 132 (8) (2010) 2555–2557.
[20] A. Iglesias-Juez, A.M. Beale, K. Maaijen, T.C. Weng, P. Glatzel, B.M. Weckhuysen, J. Catal. 276 (2) (2010) 268–279.
[21] N. Smolentsev, M. Sikora, A.V. Soldatov, K.O. Kvashnina, P. Glatzel, Phys. Rev. B 84 (23) (2011).
[22] M. Tsuda, H. Kasai, Phys. Rev. B 73 (15) (2006) 155405.
[23] T. Toda, H. Igarashi, H. Uchida, M. Watanabe, J. Electrochem. Soc. 146 (10) (1999) 3750–3756.
[24] B. Hu, N.M. Schweitzer, G.H. Zhang, S.J. Kraft, D.J. Childers, M.P. Lanci, J.T. Miller, A.S. Hock, ACS Catal. 5 (6) (2015) 3494–3503.
[25] J.T. Miller, A.J. Kropf, Y. Zha, J.R. Regalbuto, L. Delannoy, C. Louis, E. Bus, J.A. van Bokhoven, J. Catal. 240 (2) (2006) 222–234.
[26] Y.L. Yao, Y.F. Hu, R.W.J. Scott, J. Phys. Chem. C 118 (38) (2014) 22317–22324.
[27] J.R. Gallagher, D.J. Childers, H.Y. Zhao, R.E. Winans, R.J. Meyer, J.T. Miller, Phys. Chem. Chem. Phys. 17 (42) (2015) 28144–28153.
[28] X. Sang, A. Kulovits, J. Wiezorek, Acta Crystallogr. Sect. A 67 (3) (2011) 229–239.
[29] K.H.J. Buschow, P.G. van Engen, R. Jongebreur, J. Magn. Magn. Mater. 38 (1) (1983) 1–22.
[30] H.W. King, F.D. Manchester, J. Phys. F: Met. Phys. 8 (1) (1978) 15.
[31] I.V. Yudanov, R. Sahnoun, K.M. Neyman, N. Rösch, J. Hoffmann, S. Schauermann, V. Johánek, H. Unterhalt, G. Rupprechter, J. Libuda, H.-J. Freund, J. Phys. Chem. B 107 (1) (2003) 255–264.
[32] K. Wolter, O. Seiferth, J. Libuda, H. Kuhlenbeck, M. Bäumer, H.J. Freund, Surf. Sci. (Suppl. C) (1998) 402–404 428-432.
[33] J.K. Norskov, T. Bligaard, J. Rossmeisl, C.H. Christensen, Nat. Chem. 1 (1) (2009) 37–46.
[34] F. Abild-Pedersen, J. Greeley, F. Studt, J. Rossmeisl, T.R. Munter, P.G. Moses, E. Skulason, T. Bligaard, J.K. Norskov, Phys. Rev. Lett. 99 (1) (2007) 016105.
[35] M.W. Tew, J.T. Miller, J.A. van Bokhoven, J. Phys. Chem. C 113 (34) (2009) 15140–15147.
[36] S.Z. Mortazavi, A. Reyhani, A. Iraji zad, Appl. Surf. Sci. 254 (20) (2008) 6416–6421.
[37] L.D. Deng, H. Miura, T. Shishido, S. Hosokawa, K. Teramura, T. Tanaka, Chemcatchem 6 (9) (2014) 2680–2691.
[38] S. Pick, Surf. Sci. 603 (16) (2009) 2652–2657.
[39] J. Ruiz-Martínez, A. Sepúlveda-Escribano, J.A. Anderson, F. Rodríguez-Reinoso, Catal. Today 123 (2007) 235–244.
[40] J. Wu, Z. Peng, A.T. Bell, J. Catal. 311 (2014) 16l–168.
[41] R.D. Cortright, J.M. Hill, J.A. Dumesic, Catal. Today 55 (2000) 213–223.
[42] J.R. Renzas, W. Huang, Y. Zhang, M.E. Grass, D.T. Hoang, S. Alayoglu, D.R. Butcher, F. Tao, Z. Liu, G.A. Somorjai, Phys. Chem. Chem. Phys. 13 (7) (2011) 2556–2562.
[43] J.R. Renzas, W. Huang, Y. Zhang, M.E. Grass, G.A. Somorjai, Catal. Lett. 141 (2) (2011) 235–241.